ELSEVIER

Physica B 319 (2002) 233–245

PHYSICA B

www.elsevier.com/locate/physb

Evolution of magnetism and its interplay with superconductivity in heavy-fermion UPt_3 doped with Pd

Anne de Visser*

Van der Waals-Zeeman Institute, University of Amsterdam, Valckenierstraat 65, 1018 XE Amsterdam, The Netherlands

Received 14 March 2002

Abstract

The pseudobinary series $U(Pt_{1-x}Pd_x)_3$ demonstrates a wealth of magnetic and superconducting properties that are exemplary for heavy-fermion physics. In this paper, I present a survey of recent neutron-diffraction and μSR experiments, conducted to study the evolution of magnetism, and its interplay with superconductivity, in UPt_3 doped with Pd. The *small-moment antiferromagnetic* order (SMAF) with $T_N \sim 6$ K reported for pure UPt_3, is robust upon alloying till at least $x = 0.005$. The small ordered moment $m(x)$ grows from $0.018\mu_B$/U-atom for $x = 0.00$ to $0.048\mu_B$/U-atom for $x = 0.005$. T_N of the SMAF phase does not vary with Pd content. The increase of $m(x)$ correlates with the splitting ΔT_c of the superconducting transition and provides evidence for a Ginzburg–Landau scenario for *unconventional superconductivity* with magnetism as symmetry-breaking field. The absence of a signal of the SMAF phase in zero-field μSR spectra provides strong evidence for a moment fluctuating at a rate > 10 MHz. A second *large-moment antiferromagnetic* phase (LMAF) is found at higher Pd concentrations. For this phase, at optimum doping ($x = 0.05$) $T_{N,max} = 5.8$ K and $m = 0.62\mu_B$/U-atom. The critical Pd concentration for the emergence of the LMAF phase is $x_{c,af} \sim 0.006$. At the same Pd content, superconductivity is completely suppressed. The existence of a *magnetic quantum critical point* in the phase diagram, which coincides with the critical point for superconductivity ($x_{c,af} = x_{c,sc} \approx 0.006$), yields evidence for *odd-parity superconductivity mediated by ferromagnetic spin-fluctuations*.

Keywords: Magnetism; Superconductivity; Heavy fermions; UPt_3

1. Introduction

For almost two decades the intermetallic compound UPt_3 has been the subject of intense research. The strongly enhanced low-temperature specific heat, which classifies UPt_3 as a heavy-fermion compound, was reported in 1983 [1], while superconductivity in the presence of strong spin fluctuations was reported in 1984 [2]. A few years later, a multi-component superconducting phase diagram with three vortex phases in the field-temperature plane was reported [3,4]. This provided strong evidence that UPt_3 is a genuine unconventional superconductor. The subsequent explanation of the superconducting phase diagram within the Ginzburg–Landau theory of second-order phase transitions, which required an unconventional two-component superconducting order parameter (see e.g. Ref. [5]), put this on

*Tel.: +31-20-5255732; fax: +31-20-5255788.
E-mail address: devisser@science.uva.nl (A. de Visser).

0921-4526/02/$ - see front matter
PII: S0921-4526(02)01124-9

firm footing. The formation of a superconducting state in a strongly correlated metal suggests that the Cooper pairing is mediated by electronic interactions rather than by phonons. In the past decade extensive research was carried out to unravel the interplay of magnetic interactions and superconductivity in UPt_3. Here, I present a survey of recent neutron diffraction [6] and μSR experiments [7,8] conducted to study the evolution of magnetism, and its interplay with superconductivity, in the pseudobinary series $U(Pt_{1-x}Pd_x)_3$.

2. Normal and superconducting state properties of UPt_3

The low-temperature normal state of UPt_3 [1,9] presents an exemplary strongly renormalized Fermi-liquid, with a quasiparticle mass of the order of 200 times the free electron mass, as evidenced by the large coefficient of the linear term in the specific heat, $\gamma = 0.42\,\mathrm{J/molK^2}$, and the equally enhanced Pauli susceptibility, $\chi_0(T \to 0)$. The magnetic properties of this hexagonal material are quite intriguing. The magnetic susceptibility $\chi(T)$ has a broad maximum at $T_{\max} \approx 18\,\mathrm{K}$ for a field in the hexagonal plane ($B \to 0$), which is attributed to the stabilisation of antiferromagnetic interactions below $T_{\max}$. For $T < T_{\max}$ the magnetisation $M(B)$ exhibits a magnetic transition at a field $B^* = 20\,\mathrm{T}$ ($B \perp c$). This continuous phase transition has been termed pseudo-metamagnetism and is interpreted as a suppression of the antiferromagnetic interactions. The most striking magnetic property of UPt_3 is undoubtedly the small-moment antiferromagnetic phase (SMAF) which develops below the Néel temperature $T_N \sim 6\,\mathrm{K}$ [10]. The ordered moment $m = 0.02\mu_B$/U-atom is unusually small and is directed along the a^*-axis in the hexagonal plane.

Substitution studies have demonstrated that UPt_3 is close to an antiferromagnetic instability [9,11]. By replacing Pt by isoelectronic Pd, pronounced phase transition anomalies appear in the thermal and transport properties. Notably, the λ-like anomaly in the specific heat and the chromium-type anomaly in the electrical resistivity give evidence for an antiferromagnetic phase transition of the spin-density-wave type. At optimal doping (5 at% Pd) $T_{N,\max} = 5.8\,\mathrm{K}$ and the ordered moment equals $0.6 \pm 0.2\mu_B$/U-atom [6,12]. In order to distinguish this phase from the SMAF of pure UPt_3 it has been termed as the large-moment antiferromagnetic (LMAF) phase. The magnetic instability can also be triggered by substituting Th for U [13]. Remarkably, the magnetic phase diagrams for the $(U,Th)Pt_3$ and $U(Pt,Pd)_3$ pseudobinaries are almost identical. This shows that the localisation of the uranium moments is not governed by the unit cell volume of these pseudobinaries (the unit cell volume decreases by Pd doping, while it increases by alloying with Th). Long-range magnetic order also shows up when UPt_3 is doped with 5 at% Au, while substituting 5 at% Ir, Rh, Y, Ce or Os, does not induce magnetic order [14]. This indicates that a shape effect, i.e. the change in the c/a ratio, is the relevant control parameter for the occurrence of magnetic order.

Evidence has accumulated that superconductivity in UPt_3 is truly unconventional [5], i.e. the symmetry of the superconducting gap function is lower than that of the underlying Fermi surface. Evidence for this is in part presented by the power-law temperature dependence of the electronic excitation spectrum below T_c, indicating point nodes and/or line nodes in the gap [15]. UPt_3 is the only known superconductor with three different superconducting vortex phases. In zero magnetic field two superconducting phases are found, the A phase below $T_c^+ = 0.56\,\mathrm{K}$ and the B phase below $T_c^- = 0.51\,\mathrm{K}$. In a magnetic field the A phase is suppressed, while the B phase transforms into a third phase, labelled C. The three phases meet in a tetra-critical point. The phenomenology of the phase diagram has been studied extensively using Ginzburg–Landau theory, where the free energy functional is derived exclusively by symmetry arguments (the symmetry group for UPt_3 is D_{6h}). A number of Ginzburg–Landau models have been proposed [5,16] in order to explain the zero-field splitting $\Delta T_c = T_c^+ - T_c^-$ [17] and the topology of the phase diagram in magnetic field [3,4] or under pressure [18]. In the so-called E-representation model [16] the splitting ΔT_c is caused by the lifting of the degeneracy of a two-component

superconducting order parameter by a symmetry-breaking field. Substantial evidence is at hand that the SMAF phase acts as symmetry-breaking field [19,20].

3. Small-moment antiferromagnetic phase

In pure UPt_3 a small-moment antiferromagnetic phase develops below $T_N \sim 6$ K [10]. The size of the ordered moment is unusually small, $m = 0.02 \pm 0.01 \mu_B$/U-atom. The tiny moment is directed along the a^*-axis in the hexagonal basal plane. The magnetic unit cell consists of a doubling of the nuclear unit cell along the a^*-axis (see Fig. 1). In order to investigate the stability of the SMAF phase with respect to alloying, neutron-diffraction experiments have been carried out on annealed $U(Pt_{1-x}Pd_x)_3$ single-crystals with $x =$ 0.001, 0.002, 0.005 and 0.01 [6]. In order to study the effect of annealing, samples with $x = 0.001$ and 0.002 were measured before and after annealing.

The main results for $x \leqslant 0.01$ are presented in Fig. 2, which shows the temperature variation of the maximum intensity of the magnetic Bragg peak at $\mathbf{Q} = (1/2, 1, 0)$, after subtracting the background. In order to compare the size of the magnetic moments of the different samples, the intensity is expressed as m^2 in units of μ_B^2. Values of m^2 have been calculated using a systematic calibration procedure, outlined in Ref. [6].

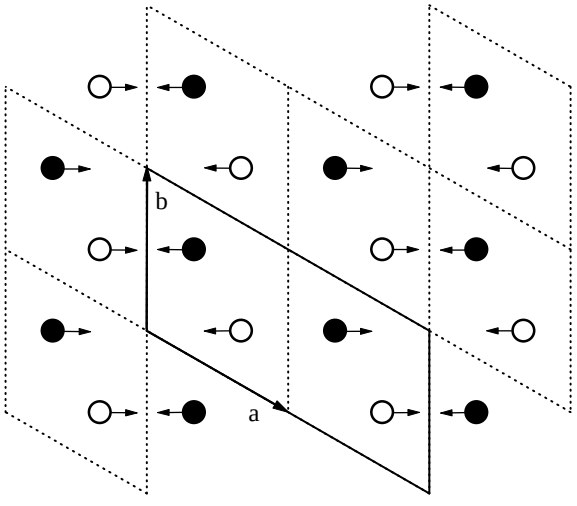

Fig. 1. Magnetic structure of $U(Pt_{1-x}Pd_x)_3$. The open (○) and closed circles (●) indicate U atoms in adjacent hexagonal planes separated by a lattice spacing $c/2$. The arrows indicate the magnetic moments, which are directed along the a^*-axis. The dotted and solid lines delineate the nuclear and magnetic unit cell, respectively.

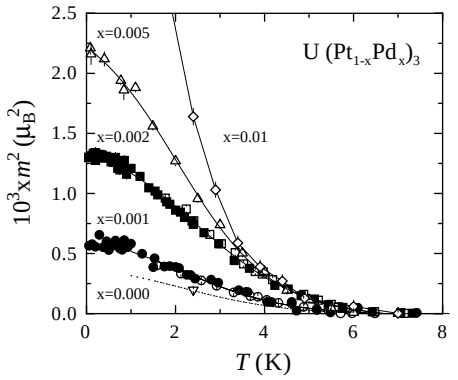

Fig. 2. Temperature variation of m^2 derived from the intensity of the magnetic Bragg peak for annealed (open symbols) and unannealed (closed symbols) $U(Pt_{1-x}Pd_x)_3$. For $x = 0.001$ (○), 0.002 (□), 0.005 (Δ) data are taken at $\mathbf{Q} = (1/2, 1, 0)$ and for $x = 0.01$ (◇) at $\mathbf{Q} = (1/2, 0, 1)$. In the case of $x = 0.00$, we have reproduced the data of Ref. [19] (----) after normalizing them to the moment deduced in Ref. [21] (▽). The solid lines are guides to the eye.

Fig. 2 clearly demonstrates that small-moment magnetism is robust upon alloying with Pd. The size of the ordered moment increases gradually with Pd concentration, but, remarkably, SMAF invariably sets in near $T_N \sim 6$ K for $x \leqslant 0.01$. For all samples with $x \leqslant 0.005$, $m^2(T)$ has an unusual form. The value of m^2 starts to rise slowly below $T_N \sim 6$ K, then a quasi-linear temperature dependence follows from ~ 4 K down to $\sim T_c$. The absolute values of the ordered moments have been calculated using integrated intensities: $m(T_c) = 0.024 \pm 0.003$, 0.036 ± 0.003 and $0.048 \pm 0.008 \mu_B$/U-atom for annealed samples with $x = 0.001$, 0.002 and 0.005, respectively. For comparison Fig. 2 shows also $m^2(T)$ for pure UPt_3, as reported in Ref. [19]. The value for $m(T_c)$ was estimated in Ref. [19] at $0.03 \pm 0.01 \mu_B$/U-atom. Because of the relatively large uncertainty in this value, $m^2(T)$ for pure UPt_3 is calibrated with help of the recent data

reported in Ref. [21]. Following the same calibration procedure as for the doped compounds, the value $m = 0.018 \pm 0.002 \mu_B$/U-atom is obtained for pure UPt_3.

The effect on annealing was investigated for the $x = 0.001$ and 0.002 samples [6]. In the limit $T \to T_c$, $m = 0.019 \pm 0.003$ and $0.038 \pm 0.003 \mu_B$/U-atom in the unannealed state, for $x = 0.001$ and 0.002, respectively. This shows that the size of the ordered moment does not change (within the experimental accuracy) by the annealing procedure. Also, the temperature variation of $m^2(T)$ does not alter upon annealing. This is illustrated by the comparison of the data for the annealed and unannealed samples shown in Fig. 2, where the moments for the unannealed sample have been multiplied by a factor of 1.26 and 0.95, for $x = 0.001$ and 0.002, respectively, for normalisation purposes. The effect of annealing on the magnetic correlation length ξ_m for $x = 0.001$ and 0.002 was also found to be negligible [6]. This is consistent with the recent conclusion reached in Ref. [22] for pure UPt_3. Since the size of the ordered moments and the values of the correlation lengths are the same within the experimental error before and after annealing, it is concluded that strain has no significant effect on the SMAF.

Zero-field μSR experiments have been performed on polycrystalline $U(Pt_{1-x}Pd_x)_3$ samples with $x = 0.000$, 0.002 and 0.005 [7]. The results for the different Pd concentrations are all very similar. Some typical muon depolarisation curves, taken on the $x = 0.005$ compound at $T = 0.1$ and 9.0 K, are shown in Fig. 3. The muon depolarization for $T < 10$ K is best described by the standard Kubo-Toyabe function, which yields an isotropic Gaussian distribution of static internal fields centred at zero field. The solid line in Fig. 3 represents a fit to the Kubo-Toyabe function for $x = 0.005$. In Fig. 4 the Kubo-Toyabe relaxation rate $\Delta_{KT}(T)$ is plotted for $x = 0.005$. For all samples, Δ_{KT} is almost temperature independent ($T < 10$ K). The average values of Δ_{KT} are 0.065 ± 0.005, 0.058 ± 0.009 and $0.083 \pm 0.004\ \mu s^{-1}$ for $x = 0.000$, 0.002 and 0.005, respectively. These values for Δ_{KT} can be attributed to the depolarisation of the muon due to static ^{195}Pt nuclear moments [7].

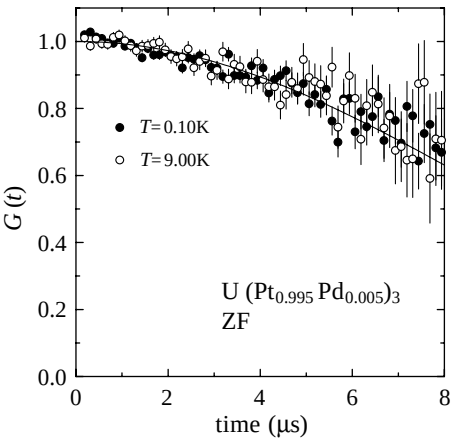

Fig. 3. Typical zero-field μSR spectra measured for polycrystalline $U(Pt_{0.995}Pd_{0.005})_3$. The solid line represents a fit to the Kubo-Toyabe function. The muon depolarisation is the same above and below the antiferromagnetic transition ($T_N \sim 6$ K).

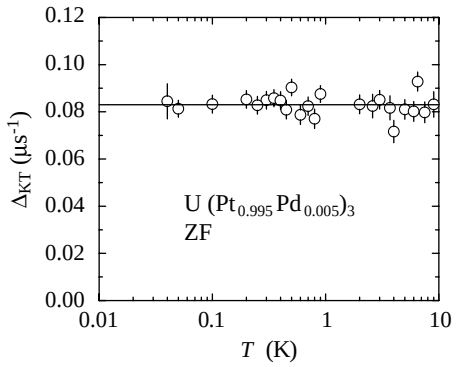

Fig. 4. Zero-field Kubo-Toyabe line width for polycrystalline $U(Pt_{0.995}Pd_{0.005})_3$. The solid line indicates the average value.

The temperature-independent behaviour of Δ_{KT} shows that the SMAF phase with $T_N \sim 6$ K does not show up in the zero-field μSR signals for $x \leqslant 0.005$. One could argue that SMAF only appears in single-crystalline samples as these were used for the neutron diffraction experiments. However, zero-field μSR experiments [23] on high-purity single-crystalline UPt_3 also do not detect the SMAF phase, while neutron-diffraction measurements carried out on parts of these samples showed that SMAF is present.

The neutron diffraction data unambiguously show that Pd doping leads to an enhancement of

SMAF, because the ordered moment grows with increasing Pd content. The reverse behaviour was observed in the neutron-diffraction experiments under pressure carried out on pure UPt_3 [19]. The moment decreases under pressure and vanishes completely at $p_c \sim 0.35$ GPa. A quite remarkable observation is that both data sets, i.e. obtained by Pd doping and applying pressure, show that T_N attains a constant value of ~ 6 K. This, together with the gradual increase of $m^2(T)$ below ~ 6 K, suggest that the transition to the SMAF state is not a true phase transition.

The origin and nature of the SMAF is still subject of lively debates. Unravelling the nature of the small moment is hampered by the fact that, till today, it has been probed convincingly by neutron-diffraction [6,11,19,21,22] and magnetic X-ray scattering [22] only. The analysis of both neutron-diffraction and magnetic X-ray scattering data [22], lead to the conclusion that SMAF is quantitatively the same in the bulk and near the surface of annealed UPt_3. The only difference is the somewhat smaller correlation length along a^* and c^* obtained in the case of magnetic X-ray scattering, $\xi_{a^*} = 85 \pm 13$ Å and $\xi_{c^*} = 113 \pm 30$ Å at $T = 0.15$ K. These values should be compared with $\xi_{a^*} = 280 \pm 50$ Å and $\xi_{c^*} = 500 \pm 130$ Å at $T = 0.57$ K in the case of the neutron diffraction experiment. These correlation lengths, although small, exclude the possibility that the SMAF is due to impurities or lattice defects. The minor influence of annealing on the SMAF, and the fact that the better samples (as determined by the degree of crystallographic order) all exhibit a magnetic moment, are in favour of an intrinsic property.

The fact that SMAF does not show up in the zero-field μSR signal strongly suggests that the small moment fluctuates in time. Absence of a μSR signal is normally explained by assuming that the muon stops at a site where the magnetic dipolar fields due to magnetic ordering cancel. However, this is highly unlikely as SMAF and LMAF have the same magnetic structure and LMAF is observed by μSR for higher Pd concentrations (see Section 4). It is also unrealistic to expect a change of the stopping site at these low Pd concentrations. The μSR technique is sensitive enough to detect a static moment of the order of $0.02\mu_B$. Therefore, one should conclude that the small moment fluctuates at a rate ($f > 10$ MHz) too fast to be detected by μSR, but on a time scale which appears static to neutrons. This then also solves the long-standing problem why SMAF of pure UPt_3 cannot be seen by NMR, whereas its signal should be much larger than the detection limit, as was concluded from NMR experiments [24] probing the LMAF phase in $U(Pt_{1-x}Pd_x)_3$ ($x = 0.05$). The absence of a true phase transition at T_N is in line with $m^2(T)$ measuring a fluctuating moment. The invariance of T_N and the crossover type of behaviour suggests that the small moment is only a weak instability of the renormalised Fermi-liquid whose properties hardly change at these low Pd concentrations ($x \leqslant 0.005$).

4. Large-moment antiferromagnetic phase

Neutron-diffraction experiments were carried out on annealed single crystals of $U(Pt_{1-x}Pd_x)_3$ with $x = 0.01$, 0.02 and 0.05 [6]. Long-range antiferromagnetic order is found with the Néel points of 1.8, 3.8 and 5.8 K, respectively. The magnetic structures for the SMAF and LMAF phases are identical. The main results are shown in Figs. 5 and 6. For $x = 0.02$ and 0.05 the

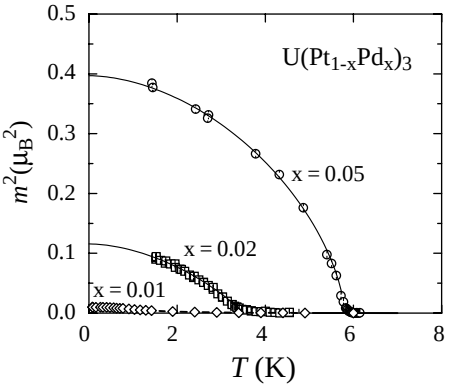

Fig. 5. Temperature variation of m^2 for annealed $U(Pt_{1-x}Pd_x)_3$ derived from the intensity of the magnetic Bragg peak $\mathbf{Q} = (1/2, 1, 0)$ for $x = 0.02$ (□) and 0.05 (○) and at $\mathbf{Q} = (1/2, 0, 1)$ for 0.01 (◇). The solid lines represent fits to $m^2(T) \propto (1-(T/T_N)^\alpha)^{2\beta}$ (see text).

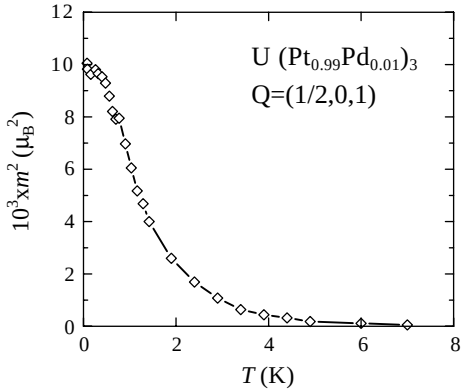

Fig. 6. Temperature variation of m^2 measured at the magnetic Bragg peak $\mathbf{Q} = (1/2, 0, 1)$ for annealed $U(Pt_{1-x}Pd_x)_3$ with $x = 0.01$ ($\diamond$). The sharp increase in the intensity near 1.8 K indicates a crossover from SMAF to LMAF.

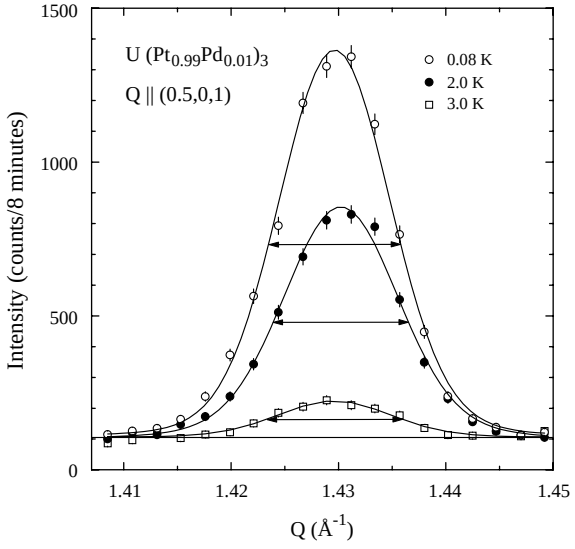

Fig. 7. Longitudinal scans of the magnetic Bragg peak $\mathbf{Q} = (1/2, 0, 1)$ for annealed $U(Pt_{0.99}Pd_{0.01})_3$ at temperatures $0.08 \leqslant T \leqslant 3$ K as indicated. The solid lines are fits to the data using a Lorentzian convoluted with the Gaussian experimental resolution. The horizontal arrows show the total width (FWHM) of the peak.

temperature variation of the maximum intensity of the magnetic Bragg peak (background subtracted) is plotted at $\mathbf{Q} = (1/2, 1, 0)$, whereas for $x = 0.01$ the magnetic intensity is plotted at $\mathbf{Q} = (1/2, 0, 1)$. Absolute values of m^2 in units of μ_B^2 have been calculated using the same calibration procedure as for the SMAF phase [6]. The temperature variation $m^2(T)$ for $x = 0.02$ and 0.05 is rather conventional compared to the quasi-linear temperature variation observed for the SMAF compounds (Fig. 2). The order parameter follows $m^2(T) \propto (1-(T/T_N)^{\alpha})^{2\beta}$, with the values $\alpha = 1.9 \pm 0.2$ and 1.8 ± 0.1 and $\beta = 0.50 \pm 0.05$ and 0.32 ± 0.03 for $x = 0.02$ and 0.05, respectively. These values of β are not too far from the theoretical value $\beta = 0.38$ for the 3D Heisenberg model [25]. The phenomenological parameter α reflects spin-wave excitations. In a cubic antiferromagnetic system α is predicted to be two [26]. No predictions are available for a hexagonal system. In the limit $T \to 0$ K, $m = 0.35 \pm 0.05$ and $0.63 \pm 0.05 \mu_B$/U-atom for $x = 0.02$ and 0.05, respectively. The size of the ordered moment obtained for $x = 0.05$ is in excellent agreement with the value reported in Ref. [12]. For the LMAF compounds the magnetic Bragg peaks are resolution limited.

The temperature dependence of the magnetic Bragg intensity of the sample with $x = 0.01$ is quite intriguing: $m^2(T)$ starts to rise slowly below $T_N \sim 6$ K, grows rapidly below ~ 2 K, and then saturates below ~ 0.5 K. The rapid rise near 2 K suggests a cross-over from the small-moment to the large-moment state, with an estimate of $T_N \sim 1.8$ K for the LMAF phase. For $T \to 0$ K, m reaches a value of $0.11 \pm 0.03 \mu_B$/U-atom. This value is obtained for both $\mathbf{Q} = (1/2, 1, 0)$ and $\mathbf{Q} = (1/2, 0, 1)$. It is emphasized that the width of the magnetic Bragg peak does not change in the temperature range 0.08–3 K (see Fig. 7), which ensures that the unusual $m^2(T)$ curve is not due to an increase of the magnetic coherence length upon lowering the temperature. Notice that for $x = 0.01$, the transition to the LMAF state does not show up in the thermal and transport data, in contrast to data for $x = 0.02$ and 0.05, which exhibit clear magnetic phase transitions at $T_N = 3.5$ and 5.8 K, respectively [9].

Zero-field μSR experiments have been performed on polycrystalline $U(Pt_{1-x}Pd_x)_3$ samples with $x = 0.01$, 0.02 and $x = 0.05$ [7]. Additional experiments on a single-crystalline $x = 0.05$ sample confirm the results obtained on the polycrystal.

For all samples we can identify a magnetic-phase-transition temperature, below which a spontaneous μ^+ precession frequency appears. This phase transition, which takes place at 1.8, 4.1 and 6.2 K for $x = 0.01$, 0.02 and 0.05, respectively, is to the LMAF state. Notice that the μSR experiments for $x = 0.01$ support the idea of a crossover from SMAF to LMAF state near $T_N \sim 1.8$ K (Fig. 6). The spontaneous μ^+ precession frequency appears only for the LMAF phase.

The μSR spectra of the three LMAF compounds below T_N have been fitted [7] with one and the same depolarization function, consisting of two terms, namely a standard depolarization function for a polycrystalline magnet, $G_v(t)$, and a Lorentzian Kubo-Toyabe function, $G_{KL}(\lambda_{KL}t)$. The Lorentzian Kubo-Toyabe term represents an isotropic Lorentzian distribution of internal fields with an average zero field. Thus, the spectral distribution of the internal fields is better approximated by a Lorentzian rather than by a Gaussian field distribution. The reason for this is not clear, and in this respect the use of the two-component depolarization function may be considered as phenomenological. In the paramagnetic state ($T > T_N$) the muon depolarization is best described by the standard Kubo-Toyabe function $G_{KT}(\Delta_{KT}t)$, just as for the SMAF compounds ($x \leqslant 0.005$), with values of Δ_{KT} comparable to the values reported in Section 3.

In Figs. 8 and 9 we show the most important parameters extracted from fitting the two-component depolarization function, namely the spontaneous frequency $v(T)$ and the depolarization rate of the Lorentzian Kubo-Toyabe function, $\lambda_{KL}(T)$, respectively. These parameters undoubtedly relate to the LMAF state, as their temperature variation obeys the same expression $f(T) = f(0)(1-(T/T_N)^{\alpha})^{\beta}$ as $m^2(T)$ (see Fig. 6), with almost identical values of α and β (see solid lines (—) in Figs. 8 and 9). A point of concern is that for a simple polycrystalline magnet one expects the spontaneous frequency $v(0)$ to scale with the ordered moment, which is clearly not the case here. Instead, $\lambda_{KL}(0)$ scales with the ordered moment. A possible reason for the absence of scaling of the frequency with the ordered moment is that the expression for $G_v(t)$ is only valid when

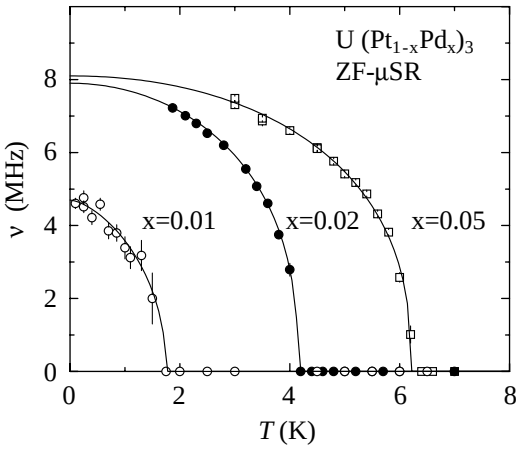

Fig. 8. Temperature variation of the spontaneous frequency v for polycrystalline $U(Pt_{1-x}Pd_x)_3$ with $x = 0.01$, 0.02 and 0.05. The solid lines represent fits to the function $f(T) = f(0)(1-(T/T_N)^{\alpha})^{\beta}$ (see text).

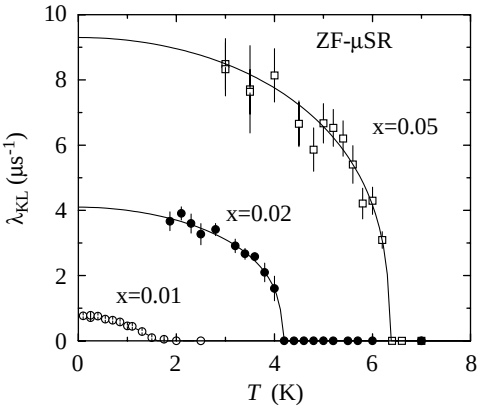

Fig. 9. Temperature variation of λKL for polycrystalline $U(Pt_{1-x}Pd_x)_3$ with $x = 0.01$, 0.02 and 0.05. The solid lines represent fits to the function $f(T) = f(0)(1-(T/T_N)^{\alpha})^{\beta}$ (see text). $\lambda_{KL}(T)$ scales with the ordered moment.

$\lambda \ll \omega = 2\pi v$. When λ is of the same order as v large systematic errors can influence the fit parameters of $G_v(t)$. Since we deal with heavily damped spontaneous oscillations this is in part the case.

5. Interplay of magnetism and superconductivity

The suppression of the double superconducting transition ($T_c^+ = 0.56$ K and $T_c^- = 0.51$ K for pure

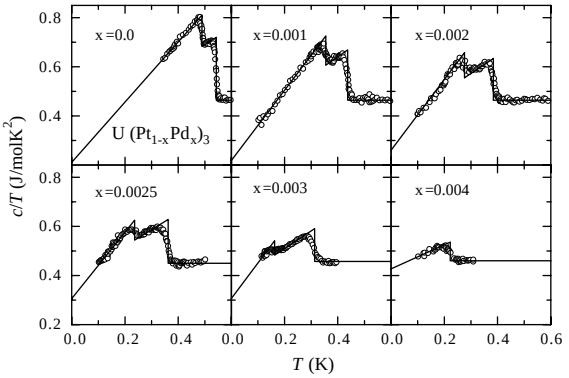

Fig. 10. Specific heat divided by T versus T of $U(Pt_{1-x}Pd_x)_3$ for $x = 0.000$, 0.001 and 0.002 (single crystals) and for $x = 0.0025$, 0.003, and 0.004 (polycrystalline samples). The solid lines represent ideal transitions determined from an equal entropy construction.

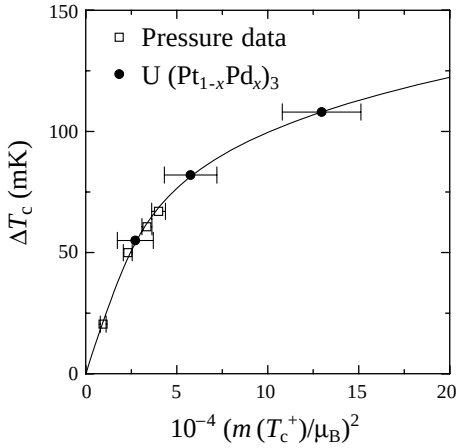

Fig. 11. The variation of the splitting ΔT_c as a function of $m^2(T_c^+)$ for $U(Pt_{1-x}Pd_x)_3$ (•) and for UPt_3 under pressure (□) [19]. For $\Delta T_c < 0.05\,K$ $\Delta T_c \propto m^2$ as predicted by the Ginzburg–Landau model. The solid line is to guide the eye.

UPt_3) as a function of Pd doping has been studied in specific heat [20] and electrical resistivity [27] experiments for a large number of single-crystalline ($x = 0.0$, 0.001, 0.002 and 0.005) and polycrystalline ($x = 0.0025$, 0.003, 0.004, 0.006 and 0.007) samples. Some exemplary specific heat data are shown in Fig. 10. The main findings can be summarised as follows: (i) T_c^+ is suppressed linearly with Pd content at a rate of $0.79 \pm 0.04\,K$/at%Pd, (ii) T_c^- is suppressed at a faster rate of $1.08 \pm 0.06\,K$/at%Pd, and as a result (iii) the splitting ΔT_c *increases* at a rate of $0.30 \pm 0.02\,K$/at%Pd. This shows that upon alloying with Pd, the high-temperature low-field A phase gains stability at the expense of the low-temperature low-field B phase. The increase in ΔT_c is accompanied by an increase in the size of the SMAF ordered moment [20]. This provides additional evidence for the idea that the SMAF acts as the symmetry-breaking field. The Ginzburg–Landau E-representation scenario [16] predicts $\Delta T_c \propto m^2$. However, this proportionality relation is only valid for $\Delta T_c/T_c \ll 1$, which no longer holds for the Pd-doped samples. At ~ 0.3 at% Pd, ΔT_c becomes of the order of T_c. Instead m^2 grows more rapidly than ΔT_c, as shown in Fig. 11. Substantial evidence for the SMAF as symmetry-breaking field has been obtained by neutron-diffraction [19] and specific heat [18] experiments under pressure. It was found that both m^2 and ΔT_c are suppressed quasi-linearly with pressure and vanish at a critical pressure $p_c \sim 0.35\,GPa$. Interestingly, a smooth variation of ΔT_c as function of m^2 is found when both the pressure and Pd doping data are plotted in one diagram (Fig. 11). This establishes a firm link between ΔT_c and m^2. Only for small splittings $\Delta T_c \propto m^2$ ($\Delta T_c < 50\,mK$). The behaviour at larger splittings evokes the need for a more sophisticated Ginzburg–Landau expansion with terms beyond the fourth order.

6. Magnetic quantum critical point near $x = 0.006$

The magnetic transition temperatures for the SMAF (Section 3) and the LMAF (Section 4) phase are plotted as a function of Pd content in Fig. 12. The magnetic phase diagram of the pseudobinaries $U(Pt_{1-x}Pd_x)_3$ shows that SMAF and LMAF are distinct phases. The differences between the SMAF and LMAF can be summarised as follows: (i) the order parameter for the SMAF is unusual and grows quasi-linearly, indicating a cross-over phenomenon, while the order parameter for the LMAF is conventional and confirms a real phase transition, (ii) T_N for the

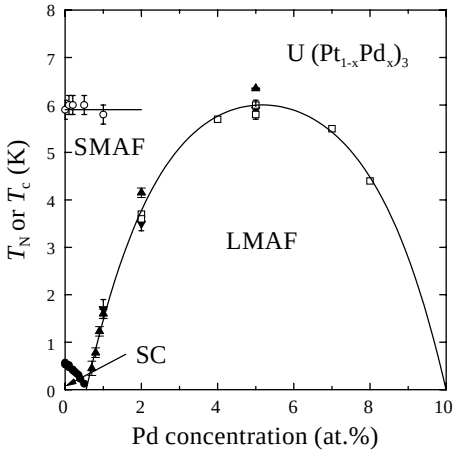

Fig. 12. Magnetic and superconducting phase diagram for $U(Pt_{1-x}Pd_x)_3$ alloys. SMAF = small-moment antiferromagnetic phase, LMAF = large-moment antiferromagnetic phase, SC = superconducting phase. The Néel temperatures T_N are measured by neutron-diffraction (○ and ▼) [6], specific heat (□) [11] and μSR (▲) [7,8]. Resistively determined superconducting transition temperatures T_c^+ (●) are taken from Ref. [27]. The solid lines are to guide the eye.

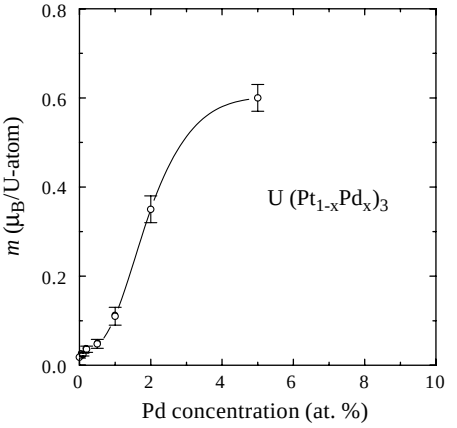

Fig. 13. SMAF and LMAF ordered moments as function of Pd concentration in single-crystalline $U(Pt_{1-x}Pd_x)_3$ alloys. The line is a guide to the eye.

SMAF does not change with Pd content (or pressure), while T_N of the LMAF compounds follows a rather conventional Doniach-type phase diagram, (iii) SMAF is not observed in zero-field μSR experiments (and NMR experiments) in contrast to LMAF. The latter point provides strong evidence that the ordered moment of the SMAF phase fluctuates at a rate $>10\,\mathrm{MHz}$. The size of the ordered moment as a function of Pd concentration is plotted in Fig. 13. The moment first increases slowly from $0.018\pm0.002\mu_B$/U-atom for pure UPt_3 to $0.036\pm0.003\mu_B$/U-atom for 0.5 at% Pd. For higher Pd concentrations ($x\geqslant0.01$) the moment rises much more rapidly. The change in slope of $m(x)$ between $x=0.005$ and $x=0.01$ is another signature that SMAF and LMAF are distinct phases.

The neutron-diffraction and μSR data presented in Sections 3 and 4 showed that T_N for the LMAF phase dropped from $\sim6\,\mathrm{K}$ for $x=0.05$ to $\sim1.8\,\mathrm{K}$ for $x=0.01$. On the other hand, for $x=0.005$, $T_N<0.04\,\mathrm{K}$ as was concluded from zero-field μSR experiments on a polycrystal down to 0.04 K [7] and single-crystal neutron-diffraction data down to 0.1 K [6]. This indicates that LMAF emerges between $x=0.005$ and 0.01. In order to determine this part of the phase diagram in more detail, transverse field ($B=0.01\,\mathrm{T}$) μSR experiments were performed on polycrystalline $U(Pt_{1-x}Pd_x)_3$ samples with $x=0.007$, 0.008 and 0.009 [8]. The μSR spectra were analysed using the damped-Gauss muon spin depolarisation function $P_{DG}(t)=A_{DG}\cos(\omega t)\exp(-\lambda_E t-\Delta^2t^2/2)$. Here, $A_{DG}\sim0.3$ is the asymmetry and $\omega=2\pi\nu_\mu$, with ν_μ the precession frequency of the muon. The Gaussian damping rate Δ is temperature independent and fixed at the observed Pt nuclear depolarization rate $\sim0.06\,\mu\mathrm{s}^{-1}$. In Fig. 14 the T dependence of the exponential damping rate $\lambda_E(T)$ is shown for all the three samples. At the highest temperatures λ_E is very small $\sim0.003\,\mu\mathrm{s}^{-1}$ and essentially T independent. Upon lowering T, λ_E increases, due to the dephasing of the muon precession frequency, which is attributed to an emerging additional source of magnetism. The additional source of magnetism becomes stronger when the Pd concentration increases, and its onset temperature is associated with the Néel temperature T_N for LMAF. Values of T_N were extracted by expressing the observed exponential damping rate as $\lambda_E=\lambda_{BG}+\lambda_{LMAF}$, where λ_{BG} and λ_{LMAF} are due to the background and the LMAF phase, respectively. λ_{BG} may account for small variations of the actual

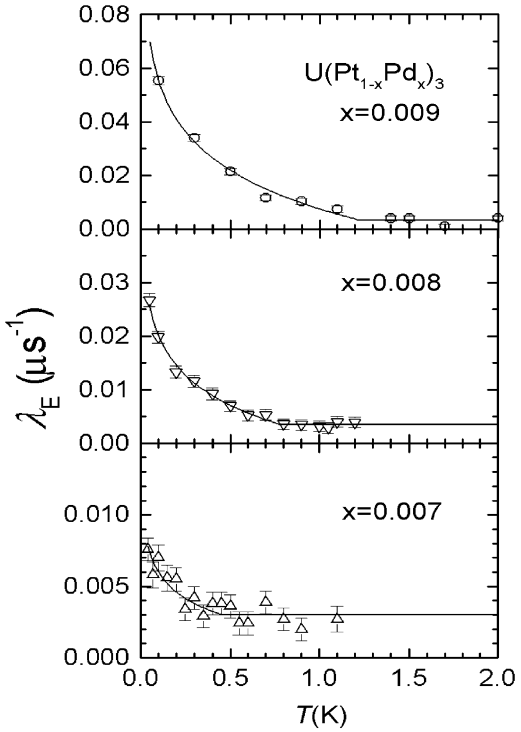

Fig. 14. Temperature variation of the exponential relaxation rate, extracted from transverse field (0.01 T) μSR spectra, for $U(Pt_{1-x}Pd_x)_3$ with $x = 0.007$, 0.008 and 0.009. The solid lines show the quasi-logarithmic increase of λ_{LMAF} below T_N and the temperature-independent background λ_{BG} above T_N.

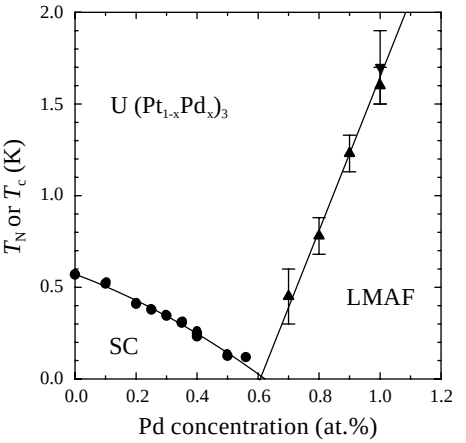

Fig. 15. Magnetic and superconducting phase diagram for $U(Pt_{1-x}Pd_x)_3$ alloys with $x < 0.012$. The meaning of the symbols is the same as in Fig. 12. The solid lines serve to guide the eye.

depolarisation rate due to Pt nuclear moments, as in the fitting procedure the fixed value $\Delta = 0.06\,\mu s^{-1}$ was used. The super-linear increase of λ_{LMAF} is unusual, and can be described phenomenologically, in this limited T interval, by a quasi-logarithmic increase $\lambda_{LMAF} \sim -\ln(T/T_N)$. Making use of this functional dependence and imposing $\lambda_{LMAF} = 0$ for $T > T_N$, the following values of T_N are extracted: 1.23 ± 0.10, 0.78 ± 0.10 and 0.45 ± 0.15 K for $x = 0.009$, 0.008 and 0.007, respectively. These values of T_N closely follow the Doniach-diagram type of behaviour obtained for $x \geqslant 0.01$ (see Section 4). Fig. 13 then shows that the LMAF phase line smoothly extrapolates to $T_N = 0$ at $x_{c,af} \approx 0.006$. The results show that it is the LMAF phase which presents the magnetic instability in $U(Pt,Pd)_3$ and not SMAF. This is consistent with recent transport measurements on polycrystalline $U(Pt,Pd)_3$ [28], which show clear deviations from Fermi-liquid behaviour in the vicinity of $x_{c,af}$, as predicted for a quantum critical point [29].

In Fig. 15 the magnetic and superconducting phase diagram is shown for $x < 0.012$. The superconducting (T_c^+) phase-transition temperatures have been taken from Ref. [27]. Inspecting the phase lines $T_N(x)$ and $T_c^+(x)$ plotted in Fig. 15, it follows that the critical concentration for the suppression of superconductivity coincides with the critical concentration for the emergence of LMAF, $x_{c,s} = x_{c,af} \approx 0.006$. The notion that the antiferromagnetic quantum critical point is not found in pure UPt_3, but is reached upon doping, may end the longstanding debate of how an odd-parity superconducting state can arise [30], while the dominant fluctuations seem to be of antiferromagnetic nature [10]. In order to resolve this controversy, it is proposed that Pd doping leads to a shift of the spectral weight from ferromagnetic to antiferromagnetic fluctuations. This idea is supported by the anomalously high rate of suppression of T_c^+ upon Pd substitution [27]. A shift of the spectral weight from ferromagnetic to antiferromagnetic fluctuations is not uncommon near a quantum critical point, where the many energy scales become comparable and competition between various phases becomes important. Indeed,

inelastic neutron scattering experiments carried out on pure UPt_3 [31] show that the magnetic fluctuation spectrum is complex and has both antiferro- and ferromagnetic components.

7. Concluding remarks

The main findings of the neutron-diffraction and μSR experiments on the pseudobinary series $U(Pt_{1-x}Pd_x)_3$ can be summarized as follows. The heavy-fermion material UPt_3 is close to an antiferromagnetic instability, however, it is the LMAF phase which represents the magnetic instability and not the SMAF phase. The critical Pd concentration for the emergence of the LMAF phase is $x_{c,af} \approx 0.006$. LMAF competes with superconductivity, as the critical concentration for superconductivity $x_{c,sc} = x_{c,af} \approx 0.006$. This suggests that superconductivity is not mediated by antiferromagnetic interactions, but rather by ferromagnetic spin fluctuations, which cannot coexist with long-range antiferromagnetic order. The SMAF phase is stable upon doping with Pd and the tiny ordered moment grows with increasing x. The increase $m(x)$ correlates with the increase of the superconducting temperature splitting ΔT_c, which provides additional evidence for a description of unconventional superconductivity with the E-representation Ginzburg–Landau scenario, where the SMAF phase provides the symmetry-breaking field. The failure to detect the SMAF phase in the zero-field μSR experiments indicates that the moment is fluctuating in time with a frequency > 10 MHz.

Clearly, the heavy-fermion properties of UPt_3 are related to the proximity to a magnetic quantum critical point. The existence of quantum critical point in the phase diagram at $x_{c,af} \approx 0.006$ is supported by a decrease of the Fermi-liquid exponent in the temperature dependence of the resistivity ($n = 2$) to a value $n \sim 1.55$ [28], i.e. close to the value $n = 1.5$ predicted [29] for an antiferromagnetic quantum critical point. Correspondingly, for the specific heat it is predicted $c \sim \gamma T - aT^{3/2}$ [29]. It would be of interest to investigate the specific heat at $x_{c,af}$. This would require high-precision specific heat data, as the effect of doping on the low-temperature specific heat is small for $x \leqslant 0.01$. For pure UPt_3, the specific heat shows a $T^3 \ln(T/T^*)$ Fermi-liquid correction term [2,9].

In the case of $U(Pt,Pd)_3$ the occurrence of LMAF can be parametrised, to a certain extent, by the reduction of the *c/a* ratio upon alloying. The application of pressure has the opposite effect, since pressure increases the *c/a* ratio due to the anisotropy in the linear compressibilities ($\kappa_c < \kappa_a$) [9]. These effects are, however, small and a satisfactory quantitative analysis is hampered by the limited accuracy in the values of the lattice constants and compressibilities. Pressure experiments, carried out on the 5 at% and 7 at% Pd samples show that doping 1 at% Pd corresponds to an external pressure of about -0.33 GPa [32]. In the case of 5 at% Pd it was demonstrated by specific heat experiments under pressure [33] that the LMAF state was fully suppressed at ~ 1.6 GPa, thereby recovering the situation at the magnetic quantum critical point. Notice that the loss of the LMAF phase near $x \sim 0.10$ (see Fig. 12) is related to changes in the crystal structure.

The nature of the SMAF phase remains puzzling. T_N is insensitive to doping and pressure, but also to strong magnetic fields (12 T) as demonstrated by neutron diffraction [21]. There is still some debate whether the SMAF phase has a single-k or triple-k structure. The high-field neutron diffraction data [21] do not support magnetic domain repopulation, which is in-line with a triple-*k* structure. However, neutron diffraction data taken under uniaxial pressure [34] support a single-*k* structure. These recent neutron scattering experiments on the SMAF phase are discussed in Ref. [35]. In the case of LMAF, the magnetic structure is single-*k*. Neutron-diffraction experiments carried out on $U(Pt_{0.95}Pd_{0.05})_3$ as function of an external field applied in the basal plane [36], showed the formation of a single-domain sample in 5 T.

Finally, whereas SMAF is not observed in zero-field μSR studies, it shows up in transverse-field studies on single-crystalline samples [37]. For a field up to 2 T directed in the basal plane two distinct and isotropic Knight shifts are observed. While the volume fractions associated with the two

Knight shifts are approximately equal at low and high temperatures, they show an opposite temperature response around $T_N \sim 6$ K. This is indicative of a decreasing fluctuation rate of the tiny moment in a magnetic field. The observation of two μSR signals of almost equal amplitude, while only one single muon stopping site has been found [38], is possibly related to the small trigonal distortion of the hexagonal lattice, recently reported in Ref. [39].

Acknowledgements

This paper is a contribution to the "*Festschrift* on the occasion of the 65th anniversary of Jaap J.M. Franse". I have enjoyed a long-term and fruitful collaboration with Jaap in the enticing field of heavy-fermion physics. On this special occasion, I would like to express my sincere gratitude to Jaap for his generous and inspiring supervision of the Magnetism and Superconductivity Research group at the Van der Waals-Zeeman Institute. The μSR and neutron-diffraction experiments described here were carried out with help of R.J. Keizer, A.A. Menovsky, B. Fåk, J.M. Mignot, P. Estrela, A. Amato, A. Schenck, C. Baines, F.N. Gygax, M.J. Graf and C.P. Opeil. I would like to thank N.H. van Dijk, A. Yaouanc and J. Flouquet for helpful discussions. This work was part of the research programme of the Dutch science foundation FOM. The ESF is acknowledged for support within the FERLIN programme.

References

[1] P.H. Frings, J.J.M. Franse, F.R. de Boer, A. Menovsky, J. Magn. Magn. Mater. 31–34 (1983) 240.
[2] G.R. Stewart, Z. Fisk, J.O. Willis, J.L. Smith, Phys. Rev. Lett. 52 (1984) 679.
[3] K. Hasselbach, L. Taillefer, J. Flouquet, Phys. Rev. Lett. 63 (1989) 93.
[4] G. Bruls, D. Weber, B. Wolf, P. Thalmeier, B. Lüthi, A. de Visser, A. Menovsky, Phys. Rev. Lett. 65 (1990) 2294.
[5] J.A. Sauls, Adv. Phys. 43 (1994) 133;
R. Joynt, L. Taillefer, Rev. Mod. Phys. 74 (2002) 235.
[6] R.J. Keizer, A. de Visser, A.A. Menovsky, J.J.M. Franse, B. Fåk, J.-M. Mignot, Phys. Rev. B 60 (1999) 6668.
[7] R.J. Keizer, A. de Visser, A.A. Menovsky, J.J.M. Franse, A. Amato, F.N. Gygax, M. Pinkpank, A. Schenck, J. Phys.: Condens. Matter 11 (1999) 8591.
[8] A. de Visser, M.J. Graf, P. Estrela, A. Amato, C. Baines, D. Andreica, F.N. Gygax, A. Schenck, Phys. Rev. Lett. 85 (2000) 3005.
[9] A. de Visser, A. Menovsky, J.J.M. Franse, Physica B 147 (1987) 81.
[10] G. Aeppli, E. Bucher, C. Broholm, J.K. Kjems, J. Baumann, J. Hufnagl, Phys. Rev. Lett. 60 (1988) 615.
[11] A. de Visser, J.C.P. Klaasse, M. van Sprang, J.J.M. Franse, A. Menovsky, T.T.M. Palstra, A.J. Dirkmaat, Phys. Lett. A 113 (1986) 489.
[12] P. Frings, B. Renker, C. Vettier, J. Magn. Magn. Mater. 63&64 (1987) 202.
[13] A.P. Ramirez, B. Batlogg, E. Bucher, A.S. Cooper, Phys. Rev. Lett. 57 (1985) 1072;
K. Kadowaki, J.J.M. Franse, S.B. Woods, J. Magn. Magn. Mater. 70 (1987) 403.
[14] B. Batlogg, D.J. Bishop, E. Bucher, B. Golding Jr, A.P. Ramirez, Z. Fisk, J.L. Smith, J. Magn. Magn. Mater. 63&64 (1987) 441;
K. Kadowaki, J.C.P. Klaasse, J.J.M. Franse, J. Magn. Magn. Mater. 76&77 (1988) 233;
K. Kadowaki, M. van Sprang, A.A. Menovsky, J.J.M. Franse, Jpn. J. Appl. Phys. 26 (Suppl. 26-3) (1987) 1243.
[15] B.S. Shivaram, Y.H. Jeong, T.F. Rosenbaum, D.G. Hinks, S. Schmitt-Rink, Phys. Rev. B 35 (1987) 5372.
[16] D.W. Hess, T. Tokuyasu, J.A. Sauls, J. Phys. Cond. Matter 1 (1989) 8135;
R. Joynt, V.P. Mineev, G.E. Volovik, M.E. Zhitomirsky, Phys. Rev. B 42 (1990) 2014;
K. Machida, M. Ozaki, Phys. Rev. Lett. 66 (1991) 3293.
[17] R.A. Fisher, S. Kim, B.F. Woodfield, N.E. Phillips, L. Taillefer, K. Hasselbach, J. Flouquet, A.L. Giorgi, J.L. Smith, Phys. Rev. Lett. 62 (1989) 1411.
[18] T. Trappmann, H. von Löhneysen, L. Taillefer, Phys. Rev. B 43 (1991) 13714.
[19] S.M. Hayden, L. Taillefer, C. Vettier, J. Flouquet, Phys. Rev. B 46 (1992) 8675.
[20] R.J. Keizer, A. de Visser, M.J. Graf, A.A. Menovsky, J.J.M. Franse, Phys. Rev. B 60 (1999) 10527.
[21] N.H. van Dijk, B. Fåk, L.P. Regnault, A. Huxley, M.-T. Fernández-Díaz, Phys. Rev. B 58 (1998) 3186.
[22] E.D. Isaacs, P. Zschack, C.L. Broholm, C. Burns, G. Aeppli, A.P. Ramirez, T.T.M. Palstra, R.W. Erwin, N. Stücheli, E. Bucher, Phys. Rev. Lett. 75 (1995) 1178.
[23] P. Dalmas de Réotier, A. Huxley, A. Yaouanc, J. Flouquet, P. Bonville, P. Imbert, P. Pari, P.C.M. Gubbens, A.M. Mulders, Phys. Lett. A 205 (1995) 239.
[24] Y. Kohori, M. Kyogaku, T. Kohara, K. Asayama, H. Amitsuka, Y. Miyako, J. Magn. Magn. Mater. 90&91 (1990) 15.
[25] C. Domb, The Critical Point, Taylor & Francis, London, 1996.
[26] R. Kubo, Phys. Rev. 87 (1952) 568.

[27] M.J. Graf, R.J. Keizer, A. de Visser, J.J.M. Franse, Physica B 259–261 (1999) 666;
M.J. Graf, R.J. Keizer, A. de Visser, A.A. Menovsky, J.J.M. Franse, Phys. Rev. B 60 (1999) 3065.
[28] M.J. Graf, R.J. Keizer, A. de Visser, S.T. Hannahs, Physica B 284–288 (2000) 1281;
C.P. Opeil, M.J. Graf, Physica B (this issue), to be published.
[29] A.J. Millis, Phys. Rev. B 48 (1993) 7183;
A. Rosch, Phys. Rev. Lett. 82 (1999) 4280.
[30] H. Tou, Y. Kitaoka, K. Asayama, N. Kimura, Y. Onuki, E. Yamamoto, K. Maezawa, Phys. Rev. Lett. 77 (1996) 1374;
Y. Dalichaouch, M.C. de Andrade, D.A. Gajewski, R. Chau, P. Visani, M.B. Maple, Phys. Rev. Lett. 75 (1995) 3938;
H.G.M. Duijn, N.H. van Dijk, A. de Visser, J.J.M. Franse, Physica B 223&224 (1996) 44.
[31] A.I. Goldman, G. Shirane, G. Aeppli, B. Batlogg, E. Bucher, Phys. Rev. B 34 (1986) 6564;
N.R. Bernhoeft, G.G. Lonzarich, J. Phys.: Condens. Matter 7 (1995) 7325.
[32] K. Bakker, Ph.D. Thesis, University of Amsterdam, 1993.
[33] J. Tang, A. de Visser, A. Matsushita, T. Matsumoto, J. Magn. Magn. Mater. 177–181 (1998) 465.
[34] N.H. van Dijk, P. Rodière, F. Yakhou, M.-T. Fernández-Díaz, B. Fåk, A. Huxley, J. Flouquet, Phys. Rev. B 63 (2001) 104426.
[35] N.H. van Dijk, P. Rodière, B. Fåk, A. Huxley, J. Flouquet, Physica B (this issue), to be published.
[36] P.H. Frings, private communication.
[37] A. Yaouanc, P. Dalmas de Réotier, F.N. Gygax, A. Schenck, A. Amato, C. Baines, P.C.M. Gubbens, C.T. Kaiser, A. de Visser, R.J. Keizer, A. Huxley, A.A. Menovsky, Phys. Rev. Lett. 84 (2000) 2702.
[38] A. Schenck, R.J. Keizer, A. de Visser, A. Amato, D. Andreica, F.N. Gygax, M. Pinkpank, P. Estrela, M.J. Graf, A.A. Menovsky, J.J.M. Franse, Physica B 289&290 (2000) 455.
[39] D.A. Walko, J.-I. Hong, T.V. Chandrasekhar Rao, Z. Wawrzak, D.N. Seidman, W.P. Halperin, M.J. Bedzyk, Phys. Rev. B 63 (2001) 054522.